Master of Science

Impact of Impurities from Spent Lithium-ion Batteries Recycling Process on NCM Precursor Morphology and Electrochemical Performance

The Graduate School of the University of Ulsan

Department of Chemical Engineering

Jae-kwon Kim

Impact of Impurities from Spent Lithium-ion Batteries Recycling Process on NCM Precursor Morphology and Electrochemical Performance

Supervisor : Professor Eun-Suok Oh

A Dissertation

Submitted to
the Graduate School of the University of Ulsan
In partial Fulfillment of the Requirements
for the Degree of

Master

by

Jae-kwon Kim

Department of Chemical Engineering

Ulsan, Korea

August 2023

Impact of Impurities from Spent Lithium-ion Batteries Recycling Process on NCM Precursor Morphology and Electrochemical Performance

This certifies that the master's thesis

of Jae-kwon Kim is approved

Committee Chair Prof. Sung-Gu Kang

Committee Member Dr. Eui-Hyuk Kwon

Committee Member Prof. Eun-Suok Oh

Department of Chemical Engineering

Ulsan, Korea

August 2023

Abstract in Korean

화석 연료 사용에 따른 기후 문제를 해결하기 위한 방안 중 하나로 많은 분야에서 리튬 이온 배터리(LIBs)의 활용이 확대되고 있다. 이에 따라 가까운 미래에는 많은 양의 폐 배터리 발생이 예상되며, 이는 또다른 환경 문제를 야기할 수 있다. 폐 배터리는 소각 또는 매립 시 토양 오염과 함께 화재 위험 등 다양한 문제를 유발할 수 있지만, 반대로 많은 양의 유가 금속을 함유하고 있어 자원으로써 재활용 가치가 높다. 따라서, 회수된 유가 금속을 이용하여 이차전지 소재인 양극 활물질을 재합성하는 기술이 주목받고 있다.

그러나 이차전지 내에는 양극 활물질의 원료가 되는 Ni, Co, Mn 외에도 집전체, 케이스, 전해질 등을 구성하는 Fe, Cu, Al, C 등 제3의 원소가 존재한다. 이러한 제3의 원소가 양극 활물질 재합성 과정에 포함되어 양극 활물질의 형상이나 구조를 변경시킬 수 있기 때문에, 이러한 불순물을 인위적으로 첨가하여 양극 활물질을 합성하는 연구가 활발히 진행되고 있다.

본 연구에서는 실제 산업 규모의 폐 배터리 재활용 공정에서 생산된 금속 용액을 분석하고, 이를 이용하여 NCM 양극 전구체 및 활물질을 합성하였다. 이를 통해 폐 배터리 재활용 과정에서 발생할 수 있는 문제와 양극 활물질 재합성에 미치는 영향을 분석하였다

ICP-OES 분석 결과, 재활용 금속 용액 내에는 예상되었던 Al, Cu와 같은

원소 외에도 재활용 공정에서 발생한 Na, Li가 많이 함유되어 있음을 확인하였다. 공침 반응을 통해 합성한 양극 전구체를 FE-SEM 분석함으로써 Na이 포함된 재활용 금속 용액을 원료로 사용한 경우엔 큰 직경의 낮은 내부 밀도 구조의 전구체가 합성되는 것을 확인하였다. 또한, XRD 분석을 통해 재활용 금속 용액으로 합성된 NCM 양극 활물질에서 더 강한 양이온 혼합이 발생한다는 것을 확인하였다.

합성한 양극 활물질의 전기화학적 성능을 평가하기 위해 2.8 - 4.25 V 전압 범위에서 150 싸이클 정전류 충방전, 출력 성능 평가, 임피던스 분석, CV 분석을 진행하였다. 기준 NCM 양극 활물질과 재활용 NCM 양극 활물질의 초기 충방전 용량에는 큰 차이가 없었으나, 50 사이클 이후, 고출력의 환경에서는 재활용 NCM 양극 활물질의 성능이 급격히 저하되는 것이 확인되었다. 이는 임피던스 분석과 CV 분석 결과를 통해 알 수 있듯이 재활용 금속 용액 내 불순물로 인한 양극 활물질의 커진 입경으로 인해 리튬 확산 거리가 길어져 charge-transfer 저항이 커진 점과 강하게 발생한 양이온 혼합으로 인한 고전압에서의 구조 불안정성 증가, 표면에 존재하는 리튬 부반응물로 인해 더 큰 polarization이 발생하였기 때문이다.

이러한 물성 분석과 전기화학적 성능 평가를 통해 폐배터리 재활용을 통한 양극 활물질 재합성시 원료 단계에서부터 정밀한 불순물 제어의 필요성을 확인하였다.

Abstract in English

The use of lithium-ion batteries (LIBs) is expanding to various fields as a solution for climate issues caused by fossil fuel. For this reason, a substantial amount of used LIBs gives another issues on how to treat in the near future, posing environmental challenges. The spent-LIBs contain valuable metals that can be utilized as resources, though they can cause problems such as soil contamination and fire hazards when incinerated or landfilled. Therefore, much attention should be given to technologies for recovering cathode active materials from the spent-LIBs.

Unfortunately, the spent-LIBs contain other elements such as Fe, Cu, Al, and C, which are called third elements, as well as Ni, Co, and Mn cathode active materials. These are components composing the collector, casing, and electrolyte. The third elements can alter the shape or structure of the cathode active material during the resynthesis process. As a result, recent research focuses on the effect of these impurities on synthesizing cathode active materials.

In this study, we analyze the metal solution produced from the spent LIBs recycling process in industry and synthesize NCM cathode precursors and active materials using this solution. We then examine potential issues which may be generated from the recycling process of waste batteries and finally investigate thoroughly the impact of the impurities on the resynthesis of the cathode active material.

The ICP-OES analysis reveals that the recycled metal solution contains a significant amount of Na and Li, which are generated during the recycling process, along with anticipated elements such as Al and Cu. FE-SEM analysis of the cathode precursor synthesized using a coprecipitation reaction confirms that the recycled metal solution containing Na produces precursor with relatively large diameter and low internal density structure. Additionally, XRD analysis reveals strong cation mixing in the NCM cathode active material synthesized from the recycled metal solution.

To evaluate the electrochemical performance of the recycled cathode active material, we conduct constant current charge and discharge for 150 cycles, impedance analysis, CV analysis, and so on. While no significant difference is observed in the initial capacity between the standard NCM and the recycled NCM, the performance of the recycled NCM is drastically deteriorated at high-output environments after 50 cycles. This phenomenon might be attributed to the increase in lithium diffusion distance because the by impurities in the recycled metal solution lead to larger diameter in the NCM size, increase structural instability at high voltages due to strong cation mixing, and finally leads to large polarization by lithium side products existing on the surface.

Through these physical and electrochemical analyses, we confirm that precise impurity control must be needed at raw material stage when resynthesizing cathode active materials from spent LIBs recycling.

Table of contents

List of figures

List of tables

CHAPTER 1. Introduction

1.1. Lithium-ion Batteries

1.1.1. Overview and Operating Principle of LIBs

Lithium-ion batteries have been widely used in various fields due to their high energy density and low self-discharge rate compared to other secondary batteries, since their proposal by M. Stanley Whittingham in the 1970s and subsequent commercialization by Sony in 1991[8]. Recently, the use of lithium-ion batteries in electric vehicles (EVs) and energy storage systems (ESS) has gained much attention to solve the problem of global warming caused by excessive fossil fuel use.

A secondary battery is a device that can convert reversible chemical energy into electrical energy. Energy conversion occurs as electrons and ions move through external circuit and electrolyte due to the potential difference between the two electrodes of the secondary battery[1]. The electrode where the spontaneous discharge reaction occurs is called the anode, and the electrode where the reduction reaction occurs is called the cathode. During discharge, electrons move from the anode to the cathode through an external circuit, while Li ions from the cathode active material pass through the electrolyte to the anode active material to convert chemical energy to electrical energy. During charge, the opposite reaction of discharge occurs under the applied voltage, converting electrical energy to chemical energy. The chemical reactions occurring at the anode and cathode are shown below.

$$\boldsymbol{Anode}: \boldsymbol{C_6 + xLi^+ + xe^- \leftrightarrow Li_xC_6}$$

$$\boldsymbol{Cathode}: \boldsymbol{Li_{1-x}MO_2 \leftrightarrow MO_2 + xLi^+ + xe^-}$$

$$\boldsymbol{Balanced\ chemical\ eqn}: \boldsymbol{C_6 + Li_{1-x}MO_2 \leftrightarrow Li_xC_6 + MO_2}$$

Lithium-ion batteries consist of four materials: cathode, anode, separator, and electrolyte. The output voltage of the battery is determined by the electrochemical potential difference between the cathode and anode. Furthermore, electrolyte and separator have a significant impact on the safety and performance of batteries. The voltage of a battery is determined by the difference in Gibbs free energy of lithium ions present in the cathode and anode, making them the primary materials responsible for determining the cell's voltage. Moreover, the cathode and anode also determine the capacity of the battery. Therefore, cathode and anode should have a spacious site for lithium ions. The electrolyte serves as a pathway for lithium-ion transport and requires high ionic conductivity. It must also electrochemical stability window in the operating voltage of the battery and maintain chemical and thermal stability during operating cell. The separator prevents physical contact between the cathode and anode, avoiding short circuits. A separator with high thermal stability can prevent battery fires. To achieve this, ceramic coating is applied, and pore control is performed to enhance the rate capability of cell[9, 10].

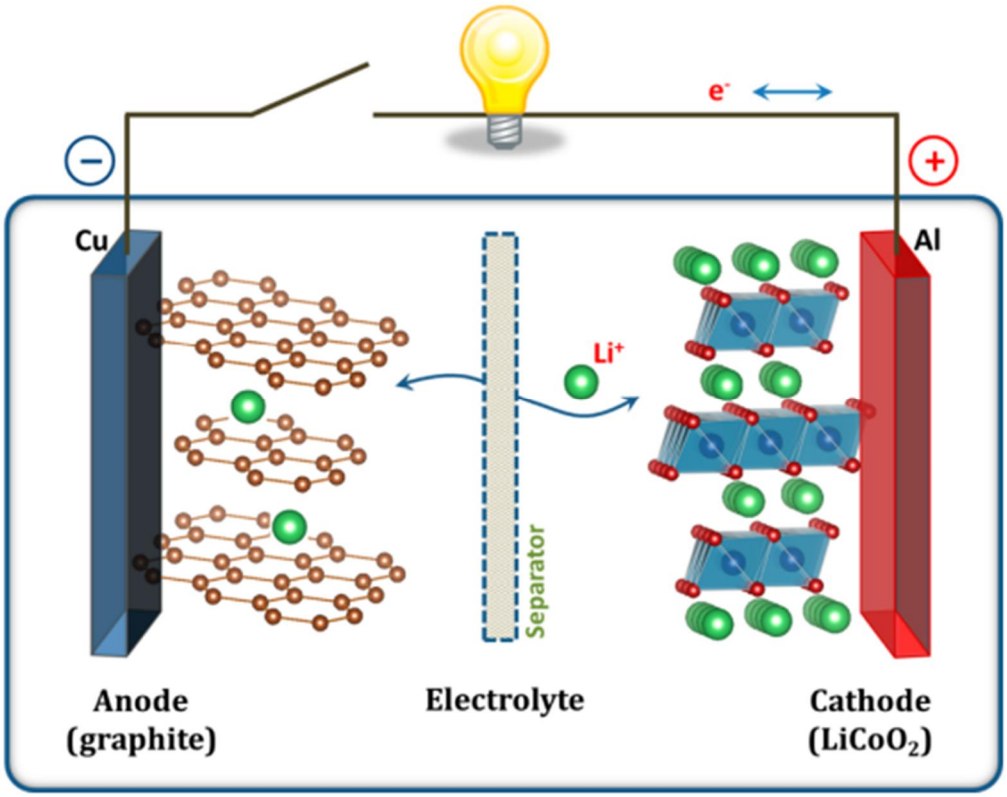

Figure 1. Schematic diagram of a Lithium-ion battery[1].

1.1.2. Cathode Materials

Cathode materials are accounting for 40% of the battery price. The output voltage of a cell is determined by the cathode, which is an important material determining the capacity of the cell, sometimes referred to as "Lithium sources." Cathode materials are classified into 3 types according to their crystal structure: polyanionic structures such as $LiFePO_4$, $Li_3V_2(PO_4)_3$, layered lithium oxide structure such as LCO, NCM, and NCA which are $LiMO_2$ $(M = Co, Ni, Mn)$, and finally, spinel structure such as $LiMn_2O_4$, $LiMn_{1.5}Ni_{0.5}O_4$[11].

The $LiFePO_4$ has the advantage of low production cost and high structure stability such that crystal structure of the fully charged state and the fully discharged state is the same. However, it has low conductivity due to one-dimensional lithium intercalation/deintercalation behavior. To compensate for this low conductivity, methods include reducing particle and grain size through hydrothermal and sol-gel processes to reduce the diffusion length of electrons and lithium ions, and carbon coating, which can improve conductivity from 10^-9 to 10^-2[12-14]. The layered structure lithium compound LCO was proposed by Goodenough and Mizushima in 1976[15]. This material achieved commercial success but faced challenges such as high production cost, instability at high temperature, and capacity degradation resulting from the extraction of more than 50% of lithium, which causes a structural transition from the hexagonal to the monoclinic phase. Subsequently, LNO was proposed as an alternative. LNO has a similar hexagonal structure and R-3m space group as LCO, allowing for easy intercalation/deintercalation. However, it has instability issues with nickel ions at high temperature. Additionally, cation mixing occurs due to the similarity in size between nickel 4+ ions and lithium ions, leading to a transition to an electrochemically inactive structure, causing capacity reduction and increased

resistance[16]. LMO also received attention for its high initial capacity of 200 mAh/g, but the high sintering temperature made synthesis challenging, and it easily transitions to the $LiMn_2O_4$ spinel structure[17]. The spinel structure provides a 3-dimensional pathway for lithium ion, resulting in faster kinetic. However, it can also cause capacity fading due to structural changes during charging. Furthermore, manganese ions can dissolve in alkyl carbonate-based organic electrolyte solution and gradually deposit on the cathode, leading to losses during charging and discharging. As a result, ternary cathode materials containing Ni, Co, and Mn were proposed. Ni contributes significantly to capacity enhancement by undergoing redox reactions from 2+ to 3+ and 3+ to 4+[18]. Cobalt helps synthesize compounds with low Ni and Li disordering and aligns the layered crystal structure, improving charging and discharging rate[19]. Manganese remains 4+ oxidation state during charging and discharging, acting as a structural stabilizer and enhancing the stability of the crystal structure[20].

Among these, layered ternary cathode materials are the most widely used due to their broad single-phase region, high capacity, reasonable production cost, and stable structure[21]. To enhance the capacity to design having long distance electric vehicles, High-Ni layered cathode materials with particularly high nickel content have been increasingly adopted. However, the high Ni content leads to issue such as cation mixing. The cation mixing causes Ni ion to substitute into the lithium ion layers, and forming NiO structure between the metal oxide layers, which hinders lithium-ion diffusion and results in a rapid capacity degradation[22, 23]. Additionally, Ni 4+ ions react with organic electrolyte consumption thereby threatening the stability of the cell. Consequently, various approaches have been attempted to prevent cation mixing, such as surface coating, element doping, and putting additives to the electrolyte[24-29]. Furthermore, research is being conducted on methods to disperse stress by controlling the concentration gradient of the

cathode material and the internal microstructure of cathode particles to prevent microcracks caused by volume changes at high voltages[30-33].

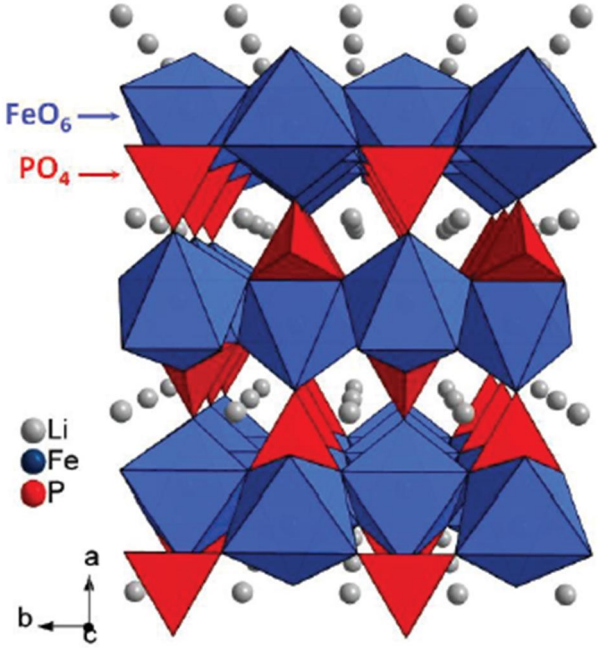

Figure 2. Olivine structure of $LiFePO_4$[2].

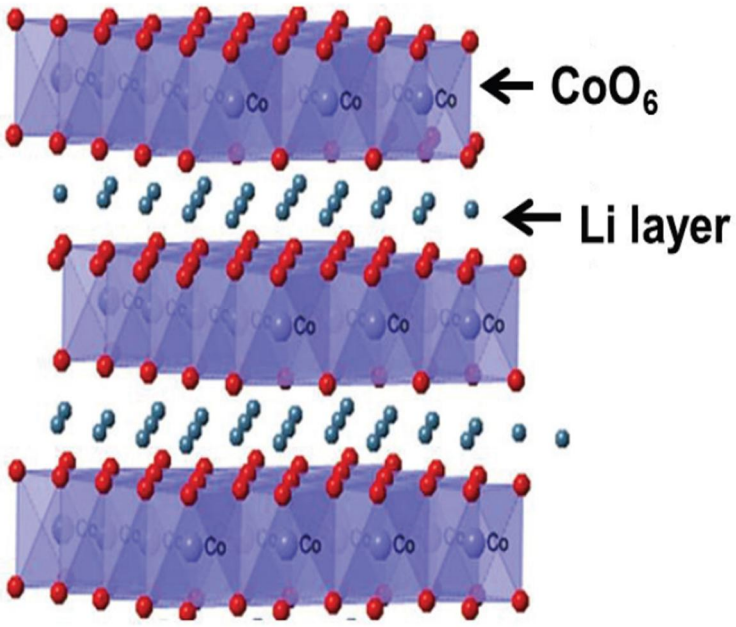

Figure 3. Layered structure of $LiMO_2$ $(M = Co, Ni, Mn)$[2].

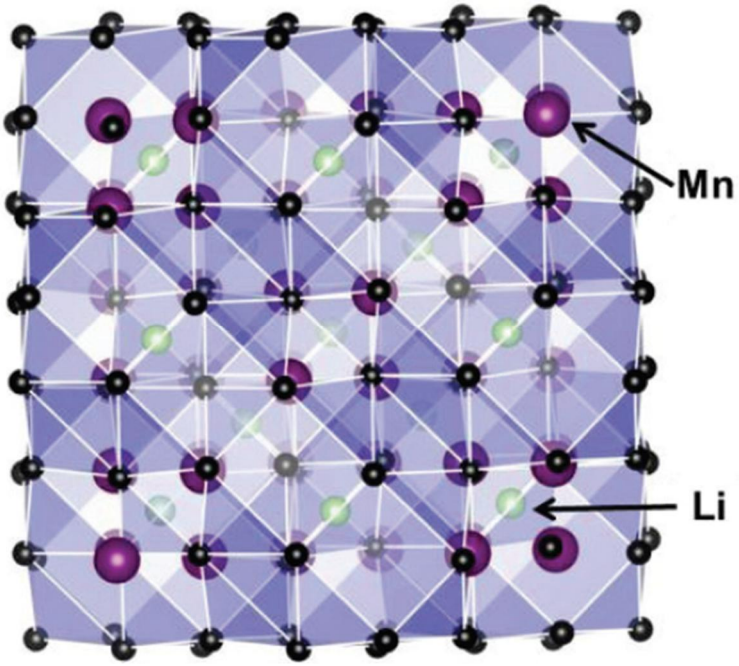

Figure 4. Spinel structure of $LiMn_2O_4$[2].

Cathode type	Chemical formula	Nominal Voltage	Operating rage	Energy density (Wh/kg)	Life cycles
Lithium Iron Phosphate(LFP)	$LiFePO_4$	3.2	2.0-3.65	90-160	2,000-7,000
Lithium Cobalt Oxide(LCO)	$LiCoO_2$	3.6	2.0-3.65	150-200	500-1,000
Lithium Manganese Oxide(LMO)	Li_2MnO_3	3.7	3.0-4.2	100-150	400-750
Lithium Nickel Cobalt Aluminium Oxide(NCA)	$LiNi_{0.8}Co_{0.15}Al_{0.05}O_2$	3.7	3.0-4.2	200-260	400-1,000
Lithium Nickel Cobalt Manganese Oxide(NCM)	$LiNi_xCo_yMn_zO_2$ *(Ni:Co:Mn=1:1:1, 6:2:2, or 8:1:1)*	3.7	3.6-4.0	160-230	2,000-3,000

Table 1. Characteristics and classification of cathode materials[4-7].

1.2. Recycling of Spent Lithium-ion Batteries

The global consumption of lithium-ion batteries is expected to significantly increase from 146.38 GWh in 2018 to approximately 439.32 GWh by 2025[34]. Consequently, the demand for raw materials needed for the production of lithium-ion batteries, as well as the market volume of spent lithium-ion batteries generated, is also expected to rise sharply[35, 36].

The most of spent lithium-ion batteries that are currently collected are buried in landfill or incinerated, but this can result in significant environmental pollution[37]. For example, spent lithium-ion batteries contain various metals such as Al, Cu, Fe, and Li that can pollute the soil, and electrolytes and separators can release harmful gases such as HF, SO_2, NO_x, HCl that can cause explosions and fires[38, 39]. Furthermore, spent lithium-ion batteries are valuable resources since they contain a large amount of rare metal and can be used to recover valuable metals with much less energy than mining for them in nature[40]. Due to the necessity and benefits mentioned above, a lot of research has been conducted recently.

There are three main methods for recycling spent lithium-ion batteries: reuse, direct recycle, and recycling for recover valuable metals. Waste batteries are gathered and graded based on their remaining lifespan. Waste batteries with a higher remaining lifespan are reused as second-life batteries[41]. The waste batteries that cannot be reused go through a pre-treatment process consisting of sorting, discharging, dismantling, deactivation, shredding, and separation to become black powder[42, 43]. Many researchers are studying the method of directly recycling the cathode active material, anode active material, and current collector separated in pre-treatment process through a few processes[44-46]. The black powder produced from the pre-treatment process is used as the raw material for LIBs recycle processes such pyrometallurgical, hydrometallurgical, or bio metallurgical which recover

metals like Li, Ni, Co, and Mn[47]. One of them, the hydrometallurgical process, recovers the valuable metal from black powder through a complex process of leaching, extraction, crystallization, and precipitation. As a result, Li, Ni, Co, and Mn in spent batteries are recovered as salts using various extraction processes[48, 49]. However, there is a concern that impurities such as Al, Cu and Mn may also be present in the leachate obtained after the acidic leaching process, along with Ni, Co, and Mn[50]. Therefore, many researchers have investigated the effect of impurities on cell performance when valuable metals such as Ni, Co, Mn from spent LIBs recycle process, that have not been fully purified, are used to synthesize active materials.[51, 52].

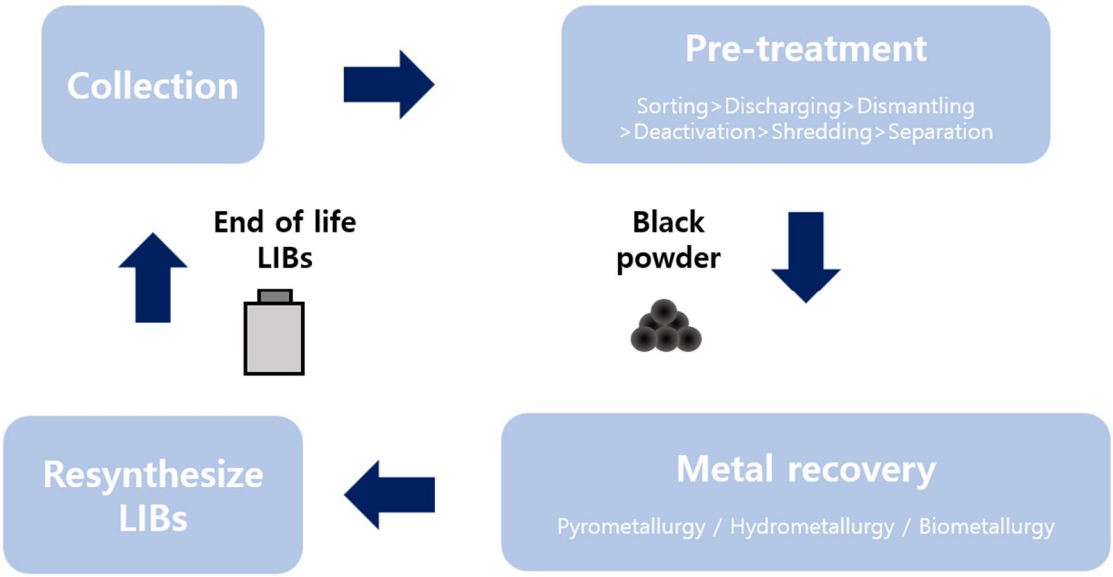

Figure 5. Schematic overview of recycling route for spent lithium-ion batteries.

1.3. Research Objectives

The popularity of lithium-ion batteries has led to a rise in discarded batteries, creating an urgent need to address the associated problems. Consequently, the recycling industry for waste batteries has rapidly expanded, leading to numerous ongoing research projects. Many of these studies specifically focus on the issue of impurities introduced during the recycling process[53-58]. These impurities can originate from various sources within the batteries, including carbon-based anode materials, Al and Cu current collectors, Fe from the cell casing, as well as chemical materials found in binders and electrolytes. These elements may not be completely separated during recycling, thus becoming impurities in the resulting cathode materials.

Unlike previous research that artificially added impurities to the metal sulfate solution for analysis, this study employs recycled metal sulfate solutions obtained from real industrial-scale battery recycling processes. These solutions serve as raw materials for co-precipitation synthesis methods in the production of precursors and cathode materials. By conducting subsequent physicochemical analyses and electrochemical evaluations, this research aims to identify potential impurities that can arise from real-world, industrial-scale waste battery recycling processes. Furthermore, it seeks to assess the impact of these impurities on the morphology of the precursors and cathode materials, as well as on the overall performance of the battery cell.

CHAPTER 2. Experiments

2.1. Synthesis of Cathode Materials

2.1.1. Co-precipitation

Co-precipitation is a method that simultaneously precipitates two or more ions from aqueous or non-aqueous solutions. This method promises homogeneous mixing of elements and produces dense particle with a narrow distribution[59]. For these reasons, it is currently the most widely used method in industrial-scale production of cathode precursor materials for lithium-ion batteries. Co-precipitation involves various process variables, such as the concentration of metal salts and chelating agent, reaction temperature, pH, and stirring speed. To synthesize high-quality precursor materials, precise control and optimization of these process variables are necessary. In addition to co-precipitation, other methods for synthesizing cathode precursor materials for lithium-ion batteries include the Sol-gel method, Hydrothermal synthesis, and spray pyrolysis[60-62].

The co-precipitation process for precursor synthesis is briefly illustrated in the Figure 6. As shown in the figure, in the co-precipitation reaction for precursor synthesis, water is supplied through a jacket to control the temperature, and nitrogen gas is continuously injected into the reactor to maintain a nitrogen atmosphere. In addition, metal ion solution, ammonia solution as a chelating agent, sodium hydroxide solution as a precipitant is injected by a peristaltic pump into the reactor to synthesize the precursor. The metal solution is prepared with a desired composition of metal compounds combined with sulfates or nitrates, and the complexing agent forms ligand ions by coordinating covalent bonding between non-shared electron pairs and metal ions, followed by the detachment of complexed NH^{3+} to combine with hydroxide ions. The chelating agent decrease the reaction

rate at which metal ions quickly precipitate with hydroxide ions, assisting in the growth of the particles. The chelating agent affects the shape and density of primary particles[63]. Since the specific pH at which precipitation occurs varies for each metal salt, an appropriate pH must be selected by referring to the Pourbaix diagram, and the synthesis mechanism of the precursor is as follows.

$$MSO_4 + 4NH_3 + 2NaOH \rightarrow M(NH_3)_4(OH)_2 + Na_2SO_4$$
$$M(NH_3)_4(OH)_2 \rightarrow M(OH)_2 + 4NH_3$$

The growth of the precursor occurs in three steps: nucleus (seed) formation, colloidal particle formation, and precipitation[3]. Ions that have reacted and been injected cluster together to form the initial nuclei of the crystals. These nuclei grow anisotropically, aggregating into plake-like primary particles grow as they attach to each other. Such growth occurs according to the Ostwald Ripening principle, where smaller particles dissolve and attach to larger particles to minimize the surface area to volume ratio and achieve a thermodynamically stable state. In this way, as the reaction time progresses, the particle takes on a spherical shape that minimizes surface energy. This growth stops when all particle sizes become equal, and the driving force of particle differences disappears. The grown particles then settle due to differences in specific gravity.

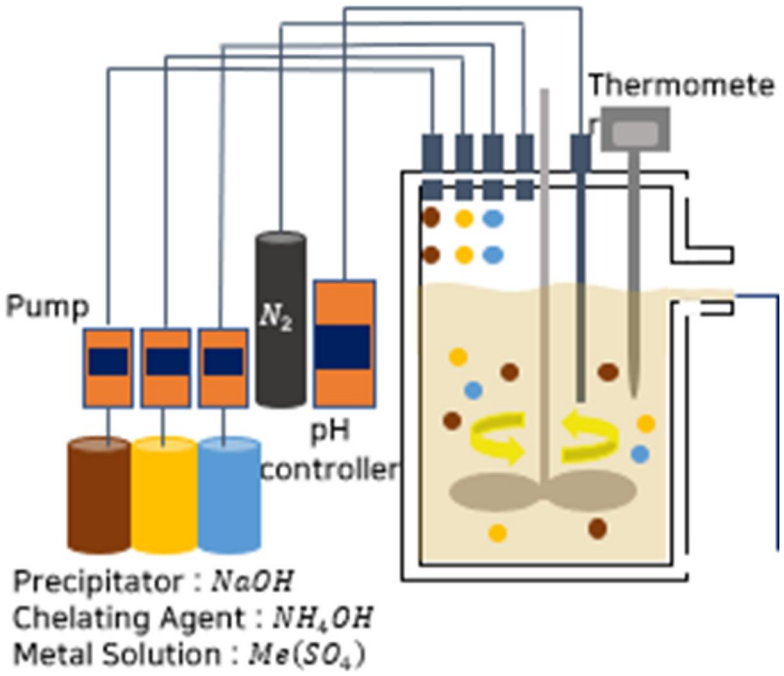

Figure 6. Facility for synthesizing precursor by co-precipitation process.

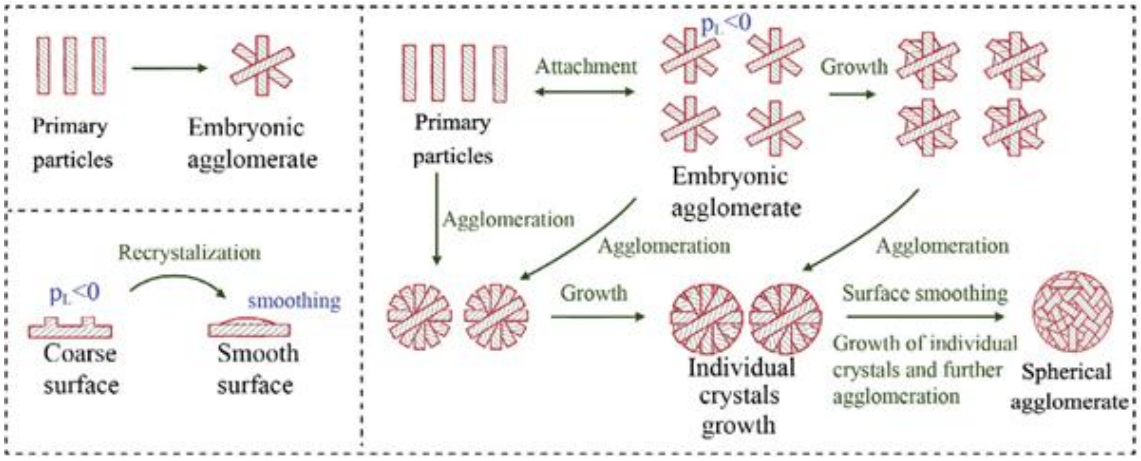

Figure 7. Schematic illustrations of the formation of particle[3].

2.1.2. Precursor Preparation

All hydroxide $(Ni_{0.6}Co_{0.2}Mn_{0.2})(OH)_2$ precursors in this work were synthesized via a hydroxide co-precipitation method and used 5 L Continuous Stirred Tank Reactor (CSTR). Nickel sulfate hexahydrate (98.5%, SAMCHUN), cobalt sulfate heptahydrate (98%, DAEJUNG) and manganese sulfate monohydrate (98%, SAMCHUN) were dissolved in DI water (molar ratio of Ni:Co:Mn=6:2:2) to form reference metal sulfate solution with a concentration of 2M. A recycled sulfate solution prepared through recycling of spent lithium-ion batteries process were provided from company. Its molar ratio and concentration were equal to the reference metal sulfate solution. In addition, sodium hydroxide (98%, SAMCHUN) and ammonia solution (28%, SAMCHUN) were dissolved in distilled water to create an aqueous solution with a concentration of 2M. After stirring overnight, the metal sulfate solutions and ammonia solution were pumped into a 5 L continuous stirred tank reactor (CSTR) at a molar ratio of 2:1 and the pH value of the reaction solution in the reactor was adjusted by feeding 2 M sodium hydroxide solution to maintain 11 at all times. The reaction process was performed under a nitrogen atmosphere, and the reaction temperature was controlled at 55 ℃. After reacting for 20h, 30h, 40h, and 50h, the hydroxide precursor was washed several times with DI water and dried in a vacuum oven for 12h at 110 ℃. The precursors obtained from the reference metal sulfate solution were abbreviated as Ref_Pre and the recycled metal sulfate solution referred to as Re_Pre.

2.1.3. Synthesis of Cathode Active Material

The dried hydroxide precursors were mixed with lithium hydroxide (98%, Sigma-Aldrich) at a molar ratio of 1:1.05 to compensate for lithium loss caused by high-temperature sintering. The mixtures were uniformly mixed by a ball-mixing method, calcined at 500 ℃ for 10h and sintered at 850℃ in air. After all these processes, the reference cathode material ($Li(Ni_{0.6}Co_{0.2}Mn_{0.2})O_2$) and recycled cathode material ($Li(Ni_{0.6}Co_{0.2}Mn_{0.2})O_2$) were successfully synthesized. Subsequently, they were designated as Ref_AM and Re_AM, respectively.

2.2. Electrode Fabrication and Cell Assembly

2.2.1. Electrode Fabrication

The slurry consisted of a uniform blend of cathode powder, carbon black (Super-P, Imerys), and poly (vinylidene difluoride (Solef PVDF 5130/1001, Solvay) that was dissolved in N-methyl-2-pyrrolidon (Sigma-Aldrich). The weight ratio was 94:3:3. The electrodes were fabricated by slurry casting on aluminum foil with a coater (MC-30, Hohsen), which was then dried for 12h at 110 . After drying, a roll press was used to compress the electrode and current collector together. To eliminate all residual water, the electrodes were dried in a vacuum oven at 110 for 10h.

2.2.2. Half Coin Cell Assembly

An argon-filled glovebox (MB200MOD, MBRAUN) (O_2, H_2O < 0.1 ppm) was used to fabricate CR-2032 size coin cells. The coin cell was composed of lithium metal (MTI Korea Co.Ltd.) as the counter electrode, a polyethylene membrane (W-Scope) as the separator, and an organic electrolyte (PuriEL, Soulbrain). The electrolyte was made of lithium hexafluorophosphate (1 M, $LiPF_6$) dissolved in a mixture of solvent ethylene carbonate (EC), ethyl methyl carbonate (EMC), and dimethyl carbonate (DMC) with a volume ratio of 1:1:1.

2.3. Materials Characterization

The inductively coupled plasma optical emission spectroscopy (ICP-OES, 700-ES, Varian) was used to compare the concentration of the metal ions in the metal sulfate solutions. The morphology, microstructure, and composition of the Precursors and cathode materials were examined by field emission scanning electron microscopy (FE-SEM, JSM-7600, JEOL and SU-8200, Hitachi) combined with energy dispersive X-ray spectroscopy (EDS). The ion milling machine (IM-4000, Hitachi) was used to observe the cross-section images of the precursors. The particle size and distribution of the precursors were verified using a particle size analyzer (PSA, LA-960, HORIBA). X-ray diffraction (XRD, ULTIMA 4, Rigaku) with Cu Kα radiation (λ=1.5406 Å) and a scan rate of 5 s/min was used to examine the phase and crystal structure of the powders. Rheological measurements of the slurry were performed using a rheometer (HR-20, TA Instruments).

2.4. Electrochemical Characterization

The electrode resistance value was obtained using an electrode resistance measurement system (RM2610, HIOKI). A battery performance evaluation system (TOSCAT-3100, Toyo system) was used to test the electrochemical performance within a voltage window of 2.8-4.25 V versus Li/Li^{+}. The cycling test, conducted to evaluate the lifespan characteristics of the battery, used current densities of 0.1 and 1C. The rate capability test, aimed at examining the battery's high-rate performance, utilized current densities ranging from 0.1 to 5C (1C=175mAh/g). Using an electrochemical analyzer (BioLogic Science Instrument, VSP-350), the cyclic voltammetry (CV) and electrochemical impedance spectroscopy (EIS) tests were

performed. The EIS test was conducted to investigate the electrochemical resistance of the cells based on their equivalent circuit models.

CHAPTER 3. Results and Discussion

3.1. ICP-OES Analysis

To investigate the differences between the Reference metal sulfate solution and Recycled metal sulfate solution, which are raw materials for the NCM precursor, we conducted ICP-OES and the results are shown in Table 2. The recycled metal sulfate solution, produced through the recycling of spent lithium-ion batteries, was found to contain a significant amount of Li and Na. This is thought to be due to the recycling process by which the recycled metal sulfate solution is produced, as shown in Figure 8.

The Hydrometallurgical treatment is the most powerful method spent lithium-ion batteries recycling process, as it has the following benefits: low energy consumption, no air emissions, and high valuable metal recovery rates. However, in the acid leaching process, sodium sulfite (Na_2SO_3) and sodium metabisulfite ($Na_2S_2O_5$) are used as reducers. This could be the reason for the high Na content in the recycled metal sulfate solution. Additionally, the fact that the Li recovery rate is not perfect from black powder during the water leaching process of Hydrometallurgical treatment is thought to be the reason for the high Li content in the recycled metal sulfate solution.

Sample	Content (mg/L)									
	Li	Na	Cr	Cu	Fe	Al	Ca	Mg	Zn	Si
Reference metal sulfate solution	**0**	**0.131**	0.127	0.164	0.004	0.006	0.346	1.8	10.4	1.54
Recycled metal sulfate solution	**1.01**	**2.13**	0.137	0.154	0.004	0.008	0.33	1.74	9.49	1.72

Table 2. Element content of Reference metal sulfate solution and Recycled metal sulfate solution.

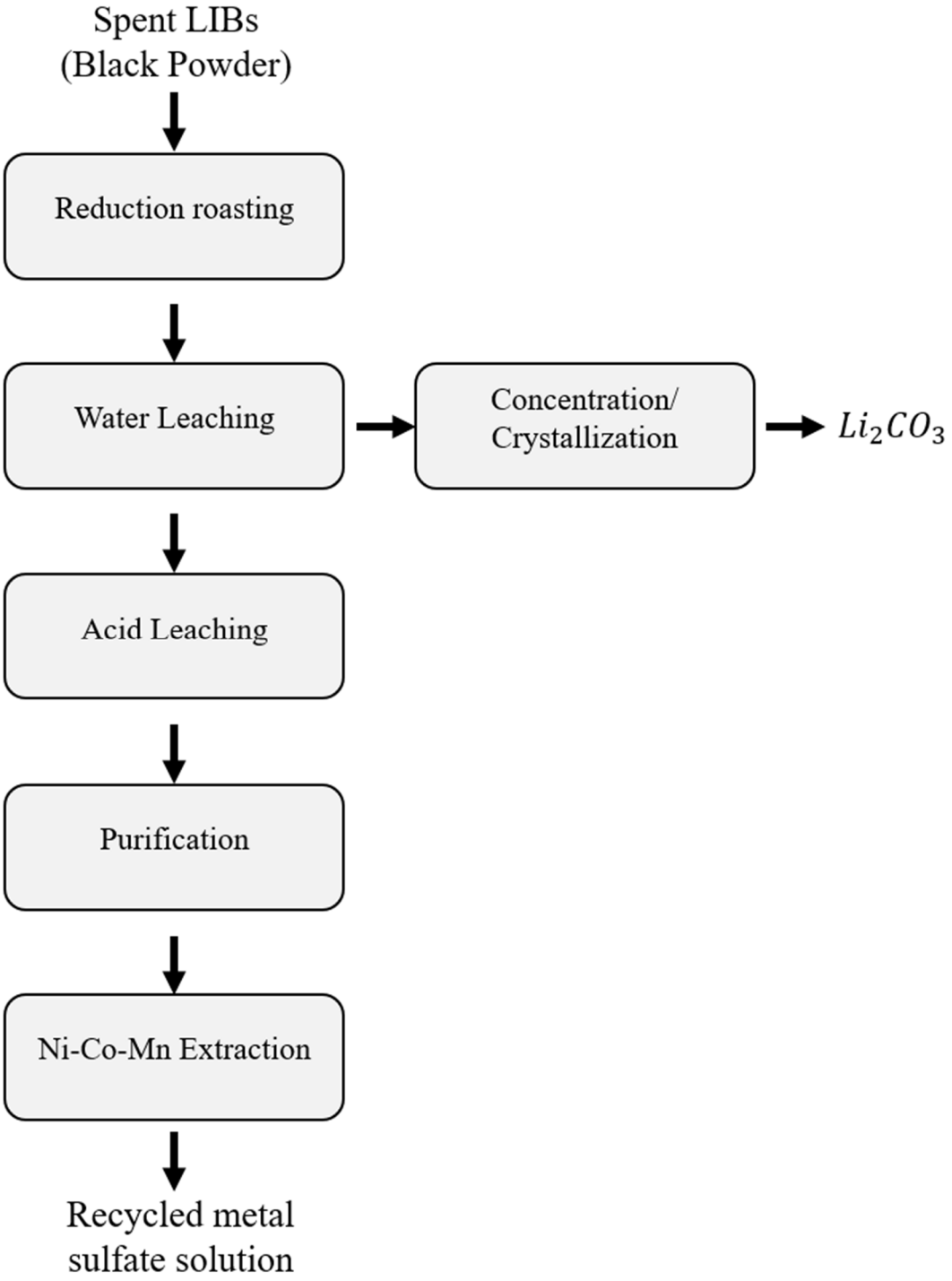

Figure 8. Schematic illustration of the process for spent lithium-ion batteries recycling.

3.2. FE-SEM/EDS Analysis

To observe the morphological changes over time in the precursors synthesized from both the Reference metal sulfate solution and the Recycled metal sulfate solution, FE-SEM analysis was conducted and depicted in Figure 9. In both cases, as the reaction progressed, it was confirmed that the spheroidization and particle growth occurred successfully according to the Ostwald Ripening principle. Furthermore, it was verified that the precursor, without any side reactions on the surface, was successfully synthesized.

Additionally, FE-SEM analysis revealed a size difference between two samples that underwent the same reaction time. To investigate this in detail, PSA analysis was conducted, and the results are presented in Table 3. As can be seen from the table, the synthesis of precursors using recycled metal sulfate solution resulted in relatively larger particles. For a more detailed analysis, an ion milling machine was used to cut the precursor, and FE-SEM analysis was conducted, which is shown in Figure 10. As can be observed in the figure, the recycled precursor exhibited numerous internal pores, leading to the formation of particles with a lower internal density. This is consistent with previous study[64], which reported that Na impurities contribute to the formation of larger particles. Therefore, it is believed that the high Na content in the recycled metal sulfate solution induced this phenomenon.

The FE-SEM/EDS analysis results of the NCM precursors cross-section in Figure 11 confirm the uniform distribution of elements of Ni, Co, Mn and the presence of a significant amount of Na in the Re_Pre and a low-density internal structure due to numerous pores.

Figure 12 shows the FE-SEM images of the NCM cathode material synthesized through the sintering process after mixing the precursor with a lithium salt. As the

basic shape and size of the cathode material are influenced at the precursor stage, spherical cathode materials like the precursor were observed. It was confirmed that Re_AM_50 h was formed with a larger size compared to Ref_AM_50 h.

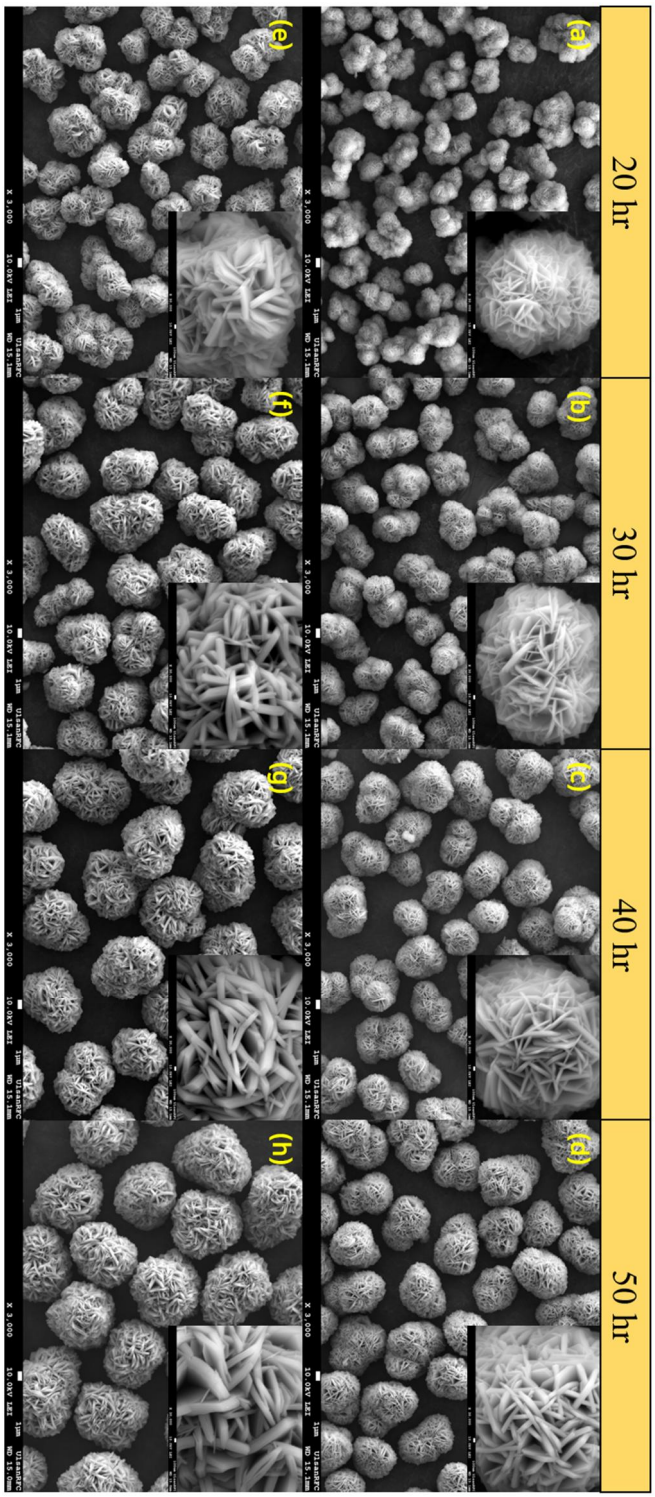

Figure 9. FE-SEM images of hydroxide precursors synthesized with different reaction time: (a)-(d) Reference precursors, (e)-(h) Recycled precursors.

	D_{10}	D_{50}	D_{90}	Span
Ref_Pre_20 h	2.1131	3.6684	5.7697	0.9968
Ref_Pre_30 h	2.2907	3.7349	5.6124	0.8894
Ref_Pre_40 h	3.0463	4.5340	6.6049	0.7849
Ref_Pre_50 h	3.1498	4.7324	7.0043	0.8145
Re_Pre_20 h	3.1080	4.5779	6.5986	0.7625
Re_Pre_30 h	3.2153	4.7690	6.9547	0.7841
Re_Pre_40 h	3.5538	5.2907	7.7995	0.8025
Re_Pre_50 h	4.1476	6.2289	9.3754	0.8393

Table 3. Particle size (μm) and span value of the precursor with reaction time.

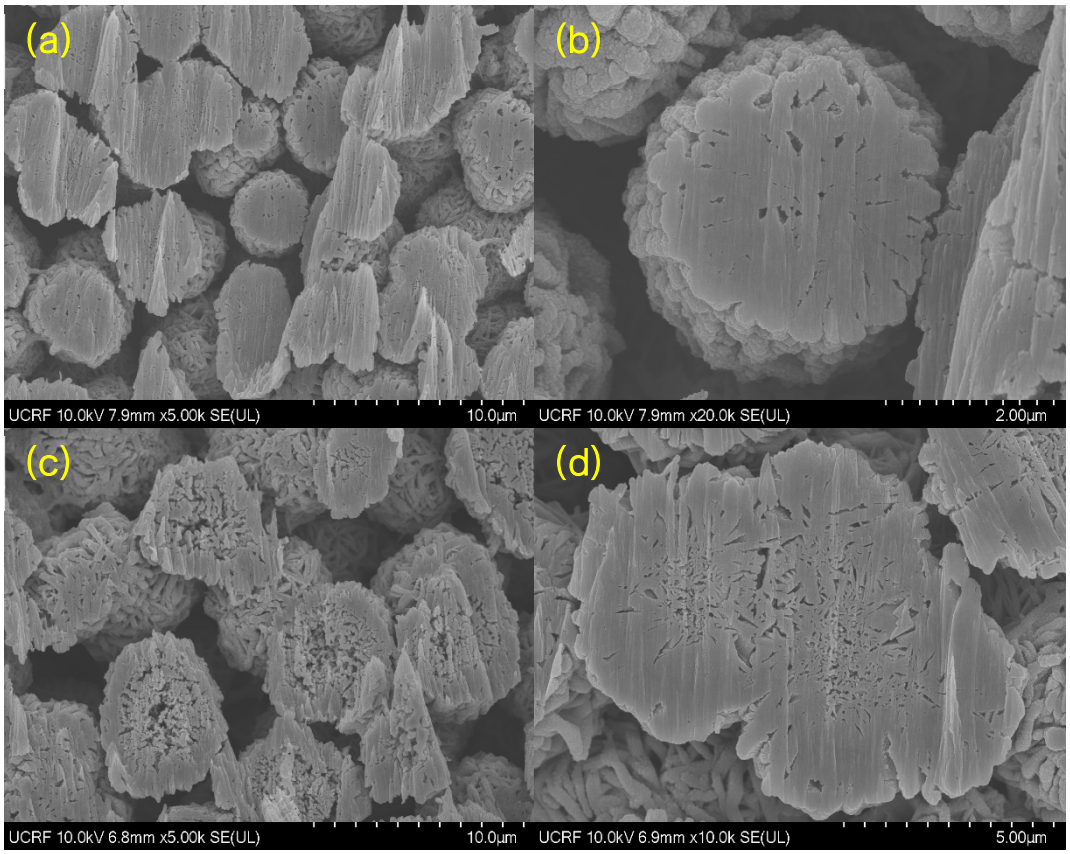

Figure 10. Cross-sectional images of the $(Ni_{0.6}Co_{0.2}Mn_{0.2})(OH)_2$ particles (a-b) Ref_Pre_50h and (c-d) Re_Pre_50h.

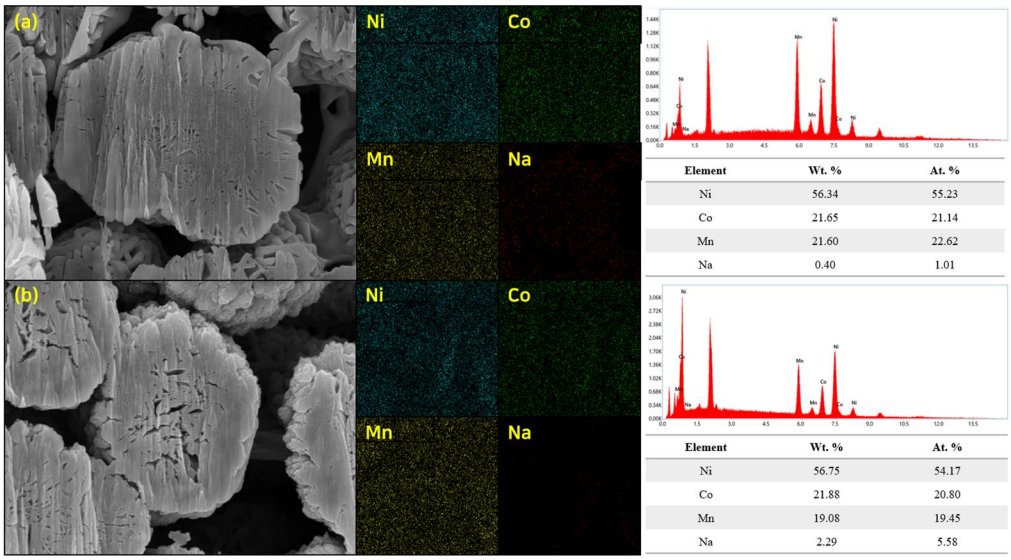

Element	Wt. %	At. %
Ni	56.34	55.23
Co	21.65	21.14
Mn	21.60	22.62
Na	0.40	1.01

Element	Wt. %	At. %
Ni	56.75	54.17
Co	21.88	20.80
Mn	19.08	19.45
Na	2.29	5.58

Figure 11. EDS spectrum and elemental mapping of Ni, Co, Mn, Na (a) Ref_Pre_50h and (b) Re_Pre_50h.

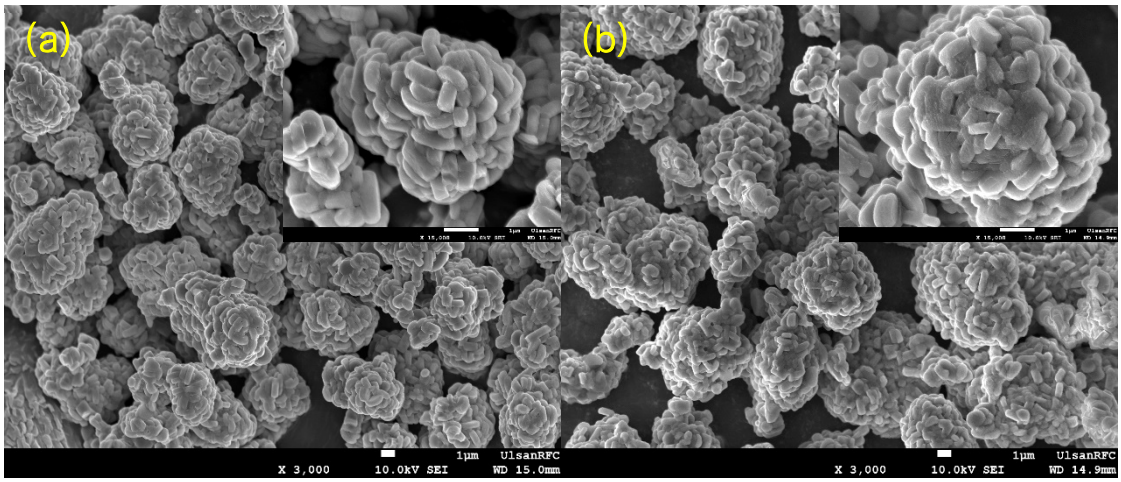

Figure 12. FE-SEM images of $Li(Ni_{0.6}Co_{0.2}Mn_{0.2})O_2$ particles (a) Ref_AM_50h and (b) Re_AM_50h.

3.3. XRD Analysis

The XRD analysis results of the synthesized cathode material are presented in Figure 13. The XRD patterns of both samples showed a hexagonal layered structure with R-3m space group and α–$NaFeO_2$ type, with no peaks indicating impurities. The clear splits of the (006)/ (102) and (108)/ (110) peaks were observed in both cases, confirming the well-formed layered structure. This showed that the impurities in the precursor had no effect on the crystal structure.

Table 4 shows the lattice parameters, c/a values, R factor, and I_{003}/I_{104} value of active materials. Some researchers have increased the c-axis by doping Na with cathode materials, taking advantage of the fact that Na ionic radius (1.02 Å) is larger than Li ionic radius (0.76 Å) to increase Li ion diffusion mobility, however in this research, a noticeable expansion of the lattice parameters and unit cell volume by Na doping was not confirmed[65]. The higher value of c/a and the lower R factor ($(I_{006}+I_{102})/I_{101}$) value is indicative of good hexagonal ordering and are known to show excellent Li diffusion ability during a charging/discharging process. Therefore, Ref_AM_50 h has a better hexagonal layered structure than Re_AM_50 h, and relatively excellent rate capability can be expected. The I_{003}/I_{104} value is known as an indicator of the cation mixing; higher value means a lower cation mixing. The Li^+, which are not located in the lithium layer due to position exchange through Ni^{2+} diffusion, reacts with CO_2 and H_2O in the air to exist on the surface of the active material in the form of surface impurities, i.e. $LiOH$ and Li_2CO_3. We confirmed, as shown in Table 4, that the influence of Li in the precursor led to higher cation mixing.

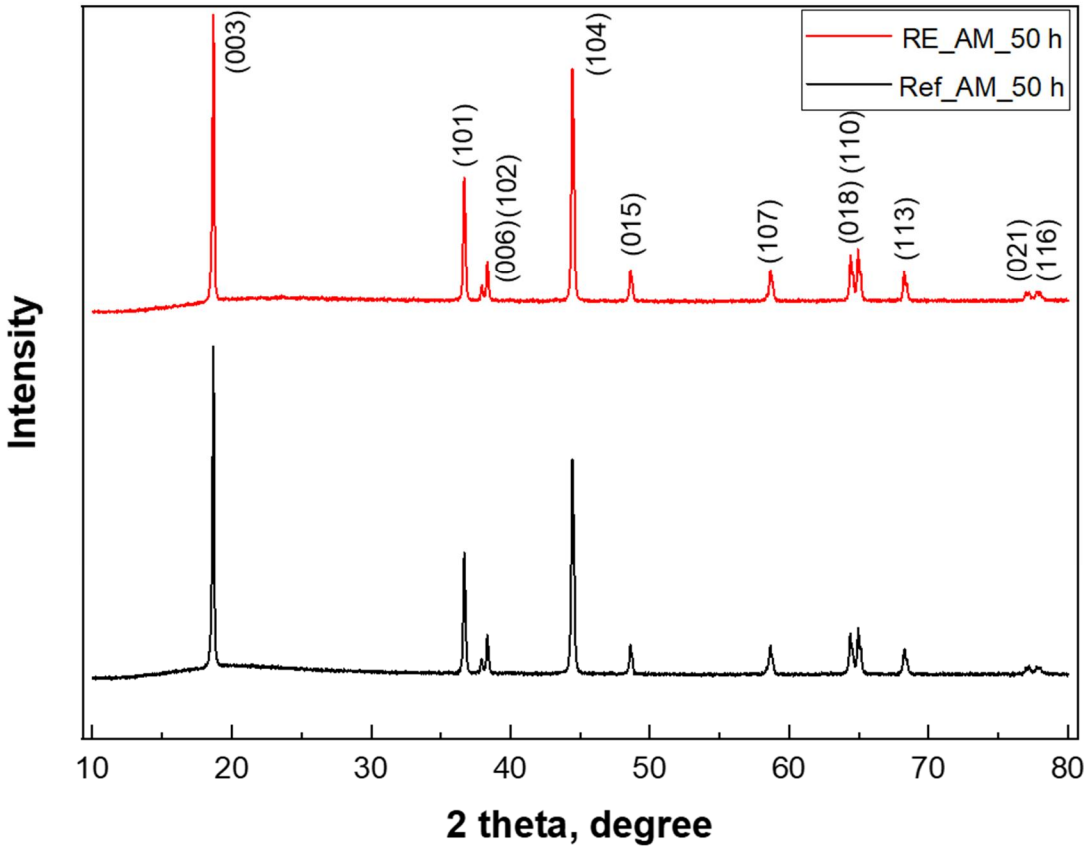

Figure 13. XRD patterns of Active materials $Li(Ni_{0.6}Co_{0.2}Mn_{0.2})O_2$.

	a (Å)	c (Å)	V(Å^3)	c/a	R factor	$I_{(103)}/I_{(104)}$
Ref_AM_50 h	2.86779	14.21904	101.27309	4.95819	0.3719	1.215
Re_AM_50_h	2.86850	14.21410	101.28867	4.95523	0.3825	1.067

Table 4. Summary of the lattice parameters of the cathode active materials.

3.4. Rheological Analysis

It is known that due to cation mixing, Li ions that are unable to position themselves within the Li layer end up residing on the surface of the cathode active material. These ions react with atmospheric H_2O, resulting in the formation of LiOH on the surface. This LiOH subsequently interacts with polyvinylidene fluoride (PVDF), a binder used in slurry production, generating H_2O, which induces slurry gelation[66]. This gelation process increases the viscosity of the slurry and impedes uniform coating.

To investigate the adverse effects of high cation mixing in Re_AM, as previously confirmed by X-ray diffraction (XRD) analysis, slurries were prepared using both Ref_AM and Re_AM, and rheological tests were performed using a rheometer. The results are presented in Figure 14. As evident from the figure, the extensive cation mixing in Re_AM resulted in the formation of residual lithium compounds on the surface, which led to slurry gelation. This gelation process increased the viscosity of the slurry, thereby serving as a barrier to uniform coating.

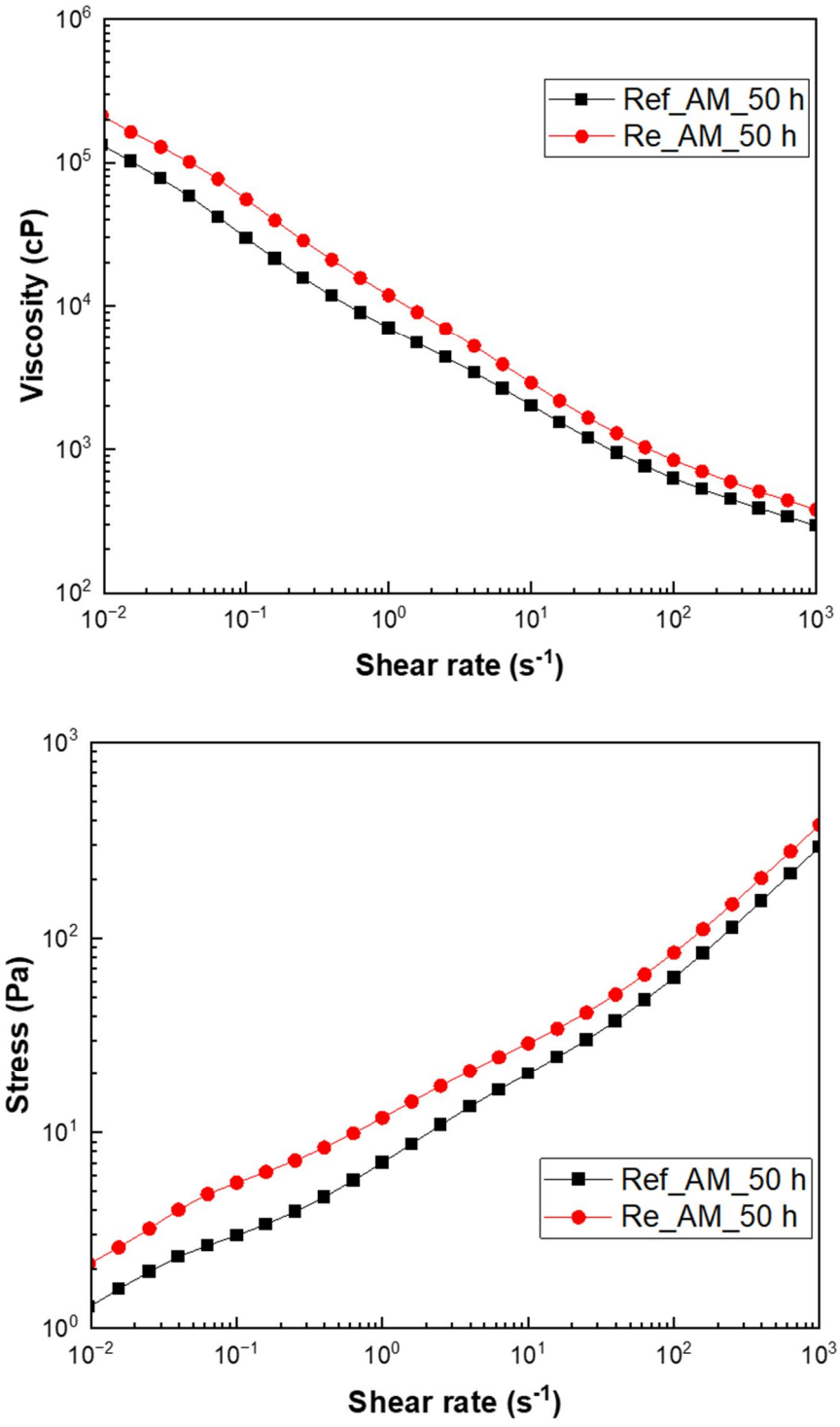

Figure 14. Rheological test results of the slurry

(a) viscosity vs. shear rate and (b) stress vs. shear rate.

3.5. Electrochemical Performance Analysis

3.5.1. Initial Charge-Discharge Capacity

The impact of sodium (Na) and lithium (Li) present in the recycled metal sulfate solution on the initial capacity of the cathode was examined by conducting initial charge and discharge at a rate of 0.1 C within a voltage range of 2.8 - 4.25 V. The initial charge and discharge capacities for Ref_AM_50 h was 171.30/170.54 mAh/g, and for Re_AM_50 h was 171.84/171.45 mAh/g, indicating no significant difference between the two. In addition, both Ref_AM_50 h and Re_AM_50 h started to show capacity at exactly 3.66 V. These findings suggest that the impurities in the metal sulfate solution do not contribute to the initial capacity degradation of the cathode.

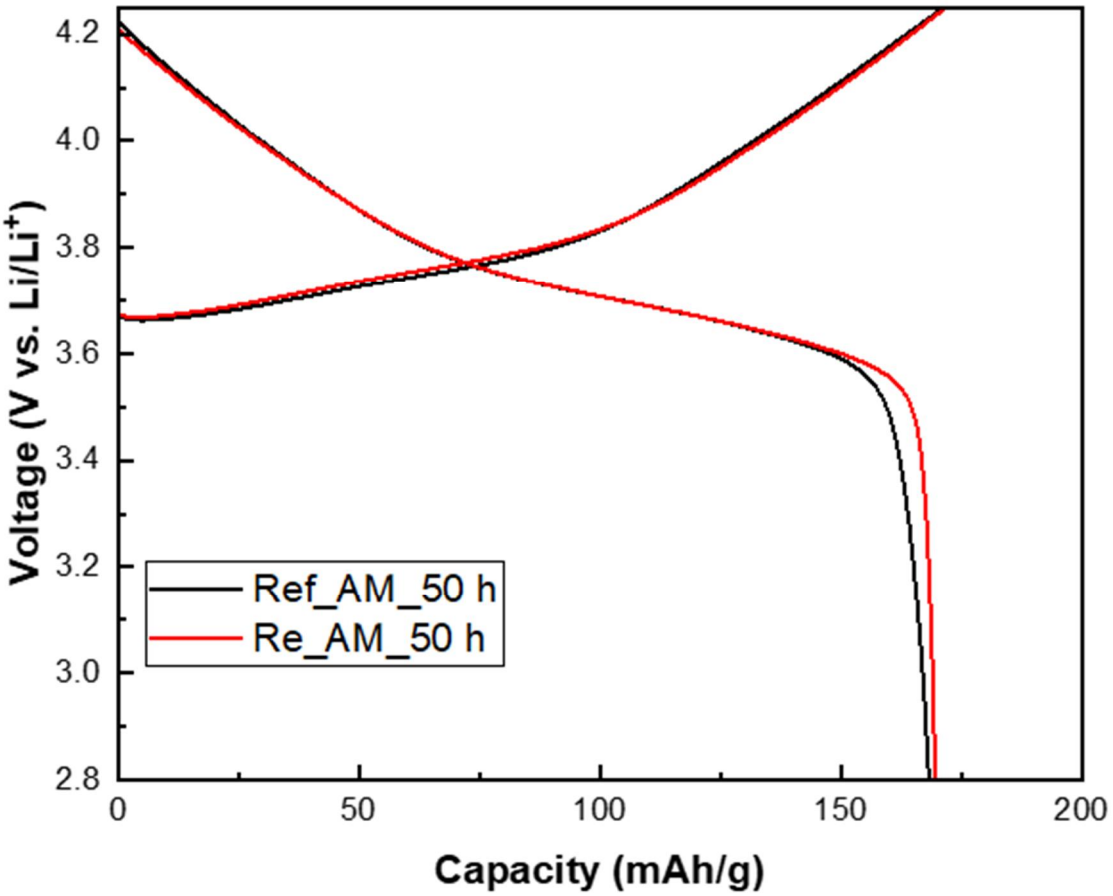

Figure 15. The initial charge-discharge curves of the samples in the voltage range of 2.8 V-4.25 V at 0.1 C at room temperature.

3.5.2. Cycling Test

In order to compare the cycling performance of the cathode in relation to the presence of impurities in the metal sulfate solution, a constant current charge and discharge was performed over 150 cycles at a current of 0.5C at 25 ℃.

Until the 50th cycles, a similar capacity decrease was observed. However, beyond this, the capacity of Re_AM_50 h sharply decreased, leading to a significant divergence. This is thought to be due to the formation of electrochemically inactive and irreversible Ni-O rock salt structures within Re_AM_50 h, resulting from the strong cation mixing previously observed in XRD analysis. These structures are believed to have obstructed the diffusion of lithium in the lithium layer[67]. On the other hand, Ref_AM_50 h, where less cation mixing occurred, exhibited excellent capacity retention.

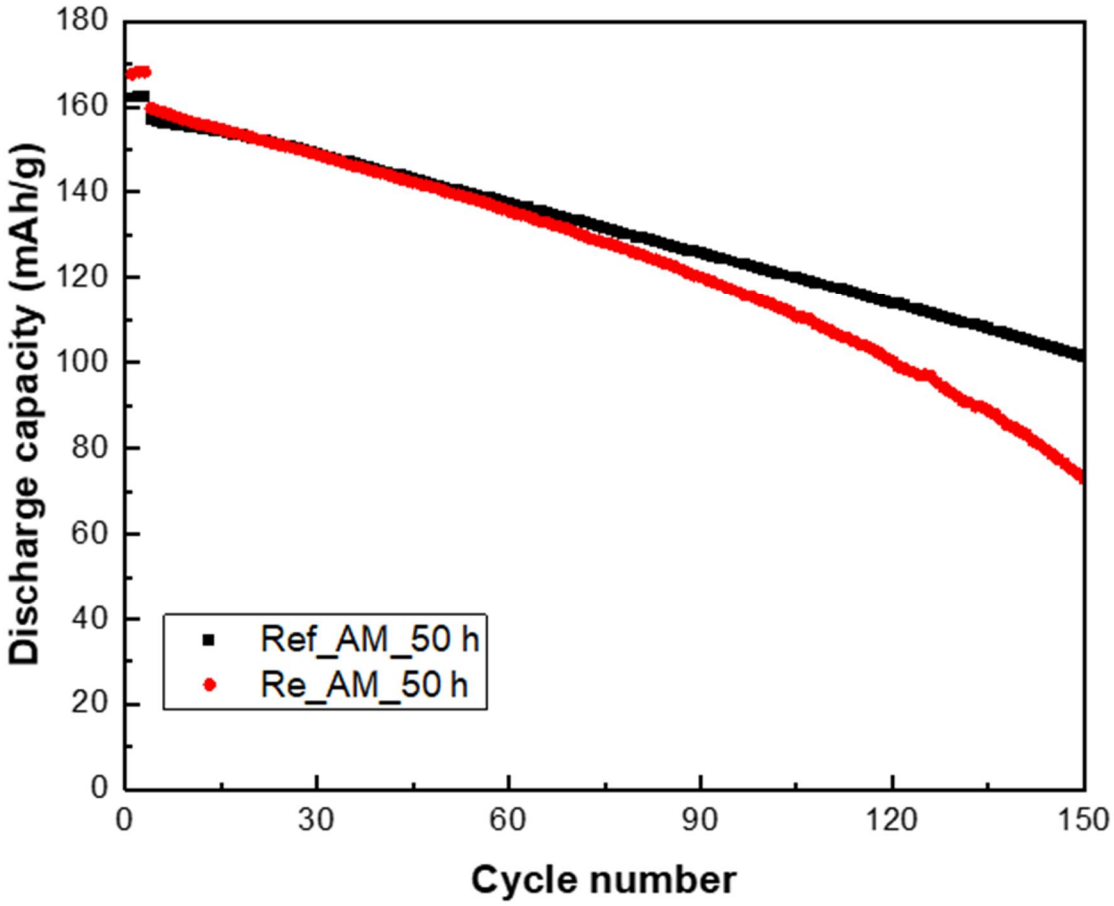

Figure 16. The cycling performance of the

Ref_AM_50 h and Re_AM_50 h at 0.5 C at 25 ℃

3.5.3. Rate Capability Test

Charge and discharge were performed at currents of 0.1 C, 0.2 C, 0.5 C, 1.0 C, 2.0 C, and 5.0 C to compare the rate capability of the cathode depending on the impurities in metal sulfate solution. As the current increased, a decline in the rate capability performance of Re_AM_50 h was observed. This is attributed to the increased lithium-ion diffusion distance due to the enlarged size of secondary particles because of the presence of sodium (Na). Moreover, the irreversible Ni-O structure caused by the strong cation mixing, triggered by the presence of lithium (Li) in the recycled metal sulfate solution, was also confirmed to contribute to the performance degradation of the cell.

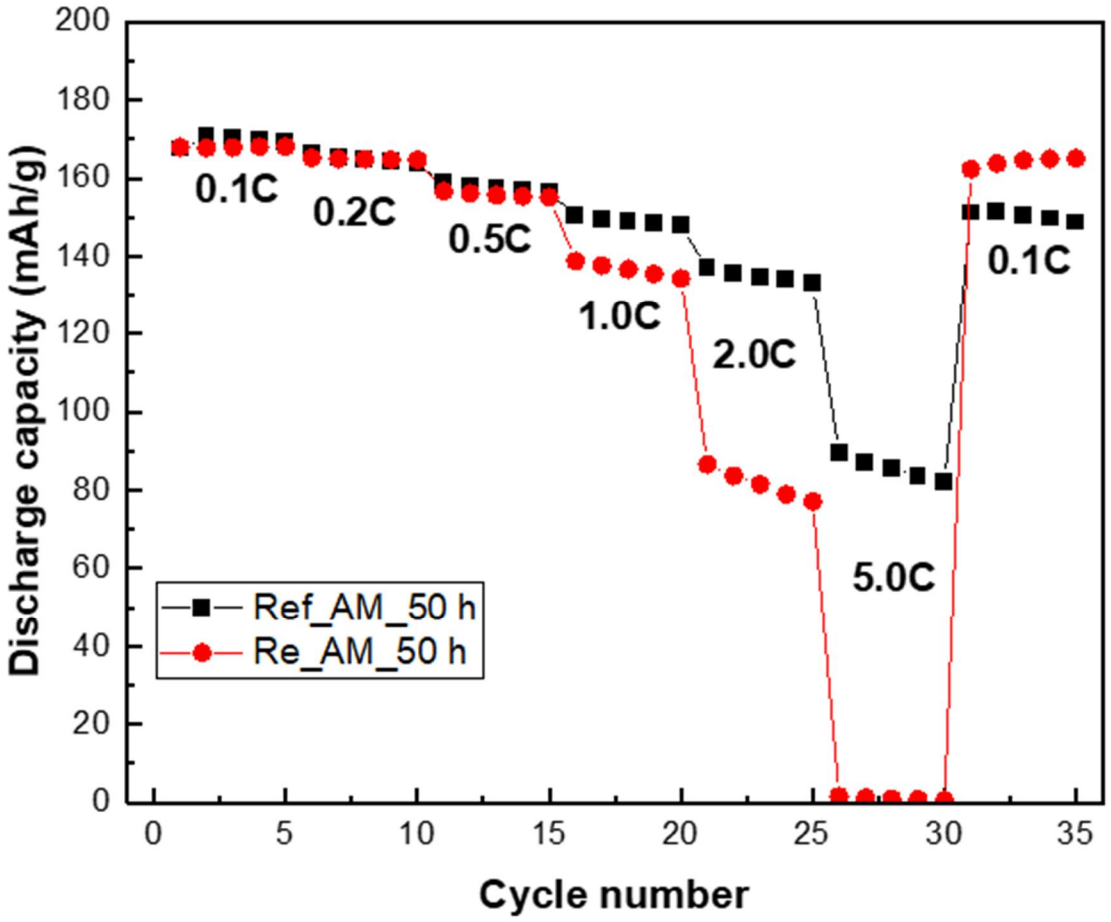

Figure 17. Rate performance of Ref_AM_50 h and Re_AM_50 h from 0.1 C to 5.0 C.

3.5.4. Cyclic Voltammetry

I utilized cyclic voltammetry to examine coin cells produced with Ref_AM_50 h and Re_AM_50 h. The analysis was conducted within a voltage range of 2.7-4.0 V at a sweep rate of 0.2 mV/s. The results are presented in Figure 18.

Typically, it is known that the redox reaction of Ni transition metal in NCM cathode materials occurs around 3.6-4.0 V[68, 69]. Through Figure 18, it can be confirmed that redox reactions occur in this range in both Ref_AM_50 h and Re_AM_50 h. Furthermore, since only one redox peak was observed in both cases, it can also be confirmed that impurities within the metal sulfate solution do not affect the electrochemical reaction of the cathode material.

Potential interval value is commonly employed to assess the polarization of electrode materials[70]. The potential interval value of Ref_AM_50 h is 0.3347V, lower than that of Re_AM_50 h which is 0.3780 V, indicating less polarization occurred in Ref_AM_50 h. This indicates that Ref_AM_50 h experienced less polarization. The greater polarization in Re_AM_50 h can be attributed to its larger particle radius, which results in a longer lithium diffusion distance, and the presence of lithium side reaction compounds on the surface. These findings align with the superior electrochemical performance demonstrated by Ref_AM_50 h in previous cycling tests and rate capability tests.

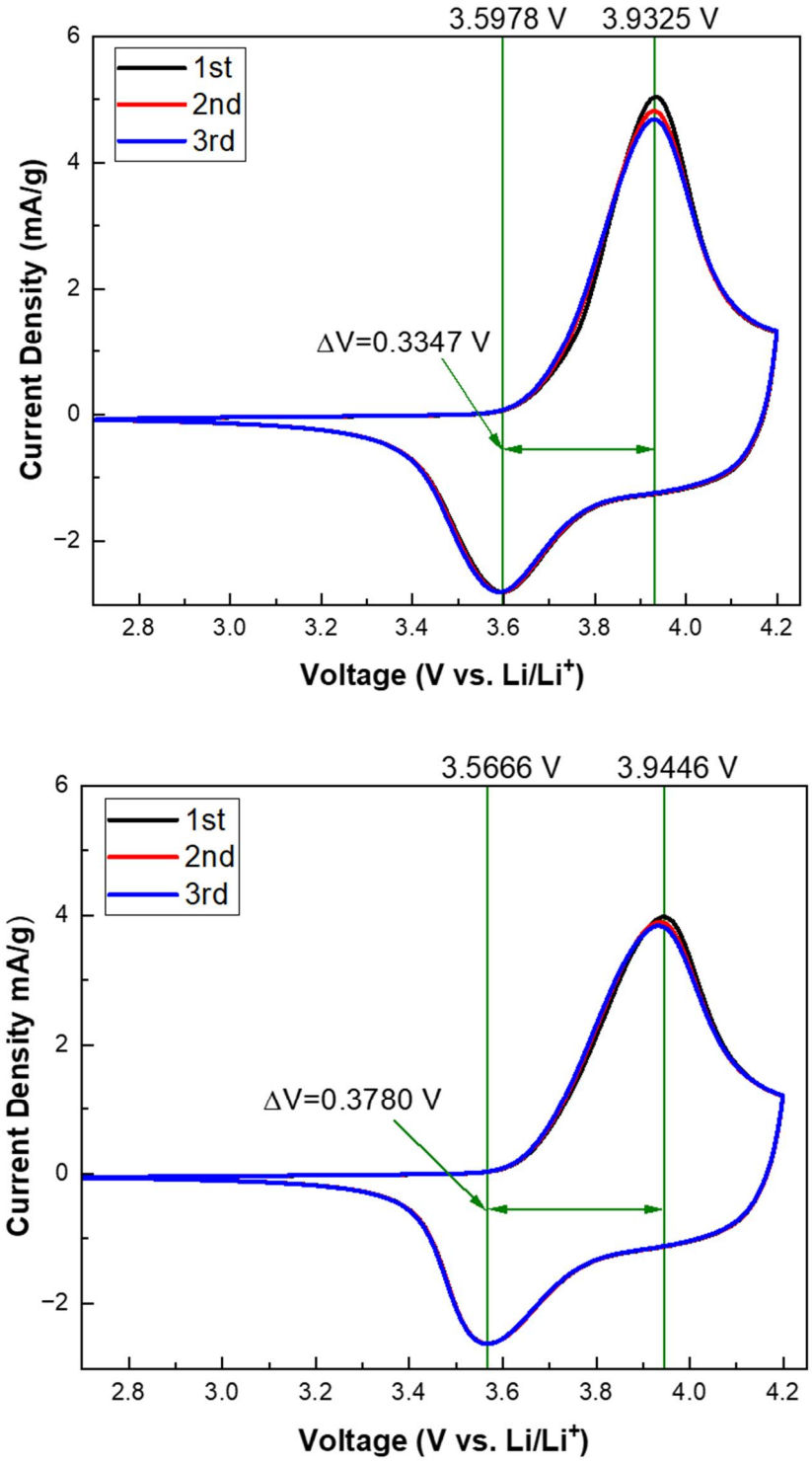

Figure 18. CV graph of the (a) Ref_AM_50 h and (b) Re_AM_50 h

3.5.5. Electrochemical Impedance Spectroscopy

To investigate the impact of impurities in the metal sulfate solution on the resistance occurring in the cathode material, conducted Electrochemical Impedance Spectroscopy (EIS) on coin cells both prior to cycling and after one cycle of charging and discharging at a current of 0.1C. The results are presented in Figure 19, using a Nyquist plot.

As can be seen in Figure 19 (a) and (b), both before and after cycling, Re_AM_50 h exhibits a higher charge transfer resistance. According another research[71], the larger the particle size of the cathode material, the greater the tendency for charge transfer resistance to increase. Re_AM_50 h, which has a larger particle size due to a low internal density precursor, is also subject to this effect, resulting in a higher charge transfer resistance. This high charge transfer resistance could account for the poor rate capability and high polarization of Re_AM_50 h.

Additionally, as noted by the Komaba group[72], a dry electrode operates like a pure electron conductor, and the resistivity of the composite electrode in the dry state can be confirmed by impedance analysis. Figure 19 (c) shows the EIS results of a dry electrode coin cell manufactured without an electrolyte. This confirms that Ref_AM_50 h has a better electronic conductivity.

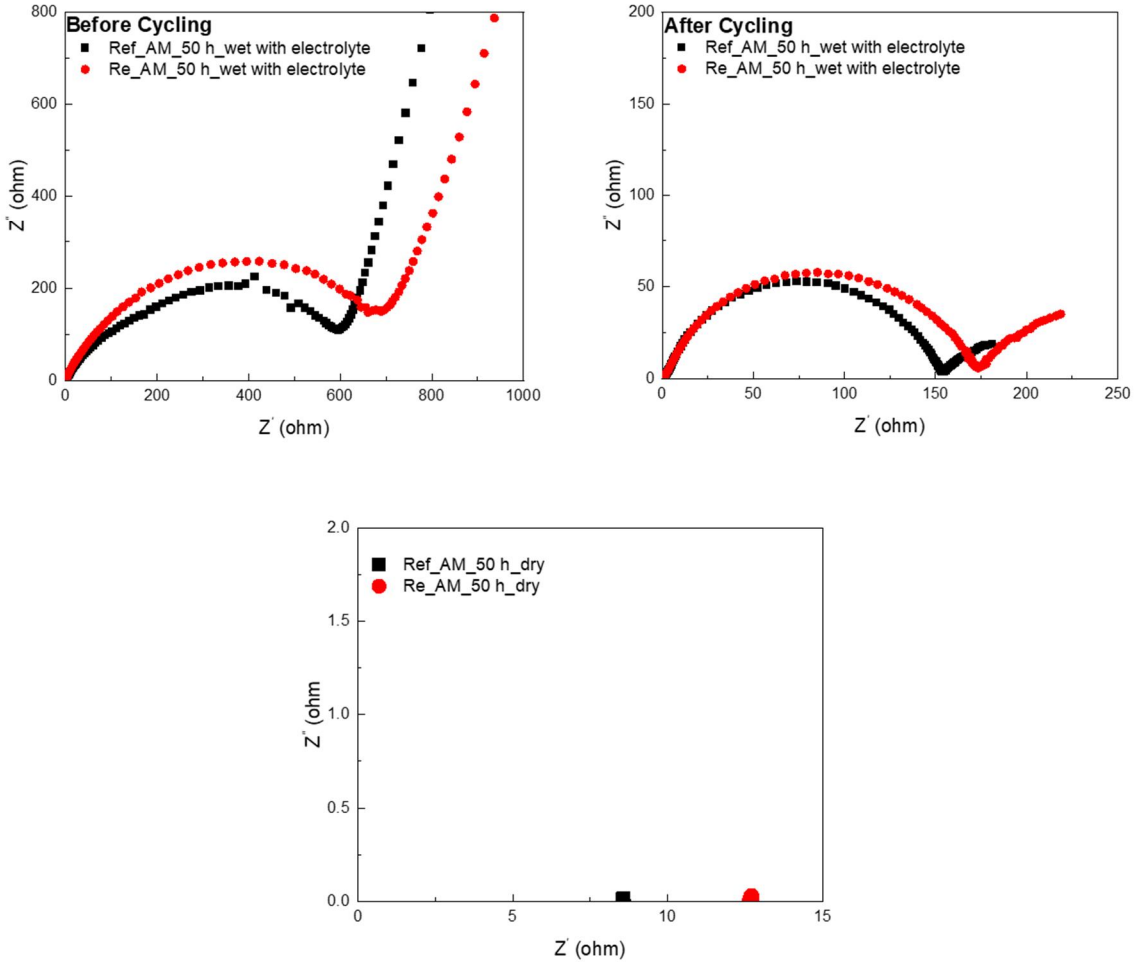

Figure 19. Electrochemical impedance spectra (EIS) of

(a) before cycling and (b) after cycling and (c) without electrolyte.

CHAPTER 4. Conclusion

This research examines the effect of potential impurities originated from the industrial-scale recycling process of spent lithium-ion batteries and analyzes their impact on the resynthesis of precursor and cathode active materials.

ICP-OES analysis confirmed the substantial presence of Na and Li ions in the Recycled Metal Sulfate Solution produced during lithium-ion battery recycling. This is attributed to the use of sodium sulfite (Na_2SO_3) and sodium metabisulfite ($Na_2S_2O_5$) as reducers during the leaching process for valuable metal recovery. It is also caused by less perfect Li recovery rate from the recycling process. The presence of Na and Li in the recycled metal sulfate solution results in the formation of precursors with less dense internal structures and induces significant cation mixing during the manufacturing process of NCM cathode. Consequently, this hinders lithium diffusion in the cathode active material, triggers gelation in the slurry, and finally leads to polarization. These detrimental effects deteriorate battery performance characteristics.

For the continued advancement of lithium-ion batteries, it is inevitable to enable the resynthesis of cathodic materials via used-battery recycling. By underscoring the necessity of impurity control in the recycling process, this study is expected to aid sustainable human development.

REFERENCES

1. Goodenough, J.B. and K.-S. Park, *The Li-ion rechargeable battery: a perspective.* Journal of the American Chemical Society, 2013. **135**(4): p. 1167-1176.
2. Daniel, C., et al. *Cathode materials review.* in *AIP Conference Proceedings*. 2014. American Institute of Physics.
3. Yang, Y., et al., *Growth mechanisms for spherical mixed hydroxide agglomerates prepared by co-precipitation method: A case of Ni1/3Co1/3Mn1/3 (OH) 2.* Journal of Alloys and Compounds, 2015. **619**: p. 846-853.
4. Chen, X., et al., *Hydrometallurgical recovery of metal values from sulfuric acid leaching liquor of spent lithium-ion batteries.* Waste management, 2015. **38**: p. 349-356.
5. Chen, Y., et al., *A review of lithium-ion battery safety concerns: The issues, strategies, and testing standards.* Journal of Energy Chemistry, 2021. **59**: p. 83-99.
6. Vonsien, S. and R. Madlener, *Li-ion battery storage in private households with PV systems: Analyzing the economic impacts of battery aging and pooling.* Journal of Energy Storage, 2020. **29**: p. 101407.
7. Sun, L. and K. Qiu, *Vacuum pyrolysis and hydrometallurgical process for the recovery of valuable metals from spent lithium-ion batteries.* Journal of hazardous materials, 2011. **194**: p. 378-384.
8. Tarascon, J.-M. and M. Armand, *Issues and challenges facing rechargeable lithium batteries.* nature, 2001. **414**(6861): p. 359-367.
9. Cho, J., et al., *High performance separator coated with amino-functionalized SiO2 particles for safety enhanced lithium-ion batteries.* Journal of Membrane Science, 2017. **535**: p. 151-157.
10. Zhang, L., et al., *High-safety separators for lithium-ion batteries and sodium-ion batteries: advances and perspective.* Energy Storage Materials, 2021. **41**: p. 522-545.
11. Zhang, S., et al., *Identifying and addressing critical challenges of high-voltage layered ternary oxide cathode materials.* Chemistry of Materials, 2019. **31**(16): p. 6033-6065.
12. Ge, Y., et al., *An optimized Ni doped LiFePO4/C nanocomposite with excellent rate performance.* Electrochimica Acta, 2010. **55**(20): p. 5886-5890.
13. Ellis, B., et al., *Synthesis of nanocrystals and morphology control of hydrothermally prepared LiFePO 4.* Journal of Materials Chemistry, 2007. **17**(30): p. 3248-3254.
14. Choi, D. and P.N. Kumta, *Surfactant based sol–gel approach to nanostructured LiFePO4 for high rate Li-ion batteries.* Journal of Power Sources, 2007. **163**(2): p. 1064-1069.
15. Mizushima, K., et al., *LixCoO2 (0< x⩽ 1): A new cathode material for batteries of high energy density.* Solid State Ionics, 1981. **3**: p. 171-174.
16. Dahn, J., U. von Sacken, and C. Michal, *Structure and electrochemistry of Li1±yNiO2 and a new Li2NiO2 phase with the Ni (OH) 2 structure.* Solid State Ionics, 1990. **44**(1-2): p. 87-97.
17. Komaba, S., et al., *Hydrothermal synthesis of high crystalline orthorhombic LiMnO2 as a cathode material for Li-ion batteries.* Solid State Ionics, 2002. **152**: p. 311-318.
18. Shaju, K., G.S. Rao, and B. Chowdari, *Performance of layered Li (Ni1/3Co1/3Mn1/3) O2 as cathode for Li-ion batteries.* Electrochimica Acta, 2002. **48**(2): p. 145-151.
19. Whitfield, P., et al., *Investigation of possible superstructure and cation disorder in the lithium battery cathode material LiMn1/3Ni1/3Co1/3O2 using neutron and anomalous*

dispersion powder diffraction. Solid State Ionics, 2005. **176**(5-6): p. 463-471.
20. Reed, J. and G. Ceder, *Charge, Potential, and Phase Stability of Layered Li (Ni0. 5Mn0. 5) O 2.* Electrochemical and solid-state letters, 2002. **5**(7): p. A145.
21. Li, X., et al. *Research Status of Ni-rich Ternary Cathode Materials for Lithium Ion Batteries*. in *IOP Conference Series: Earth and Environmental Science*. 2020. IOP Publishing.
22. Wang, F. and J. Bai, *Synthesis and Processing by Design of High Nickel Cathode Materials.* Batteries & Supercaps, 2022. **5**(1): p. e202100174.
23. Zhang, H., et al., *Single Crystalline Ni Rich LiNixMnyCo1− x− yO2 Cathode Materials: A Perspective.* Advanced Energy Materials, 2022: p. 2202022.
24. Zhang, X.-D., et al., *An effective LiBO2 coating to ameliorate the cathode/electrolyte interfacial issues of LiNi0. 6Co0. 2Mn0. 2O2 in solid-state Li batteries.* Journal of Power Sources, 2019. **426**: p. 242-249.
25. Shan, W., et al., *Surface coating for high-nickel cathode materials to achieve excellent cycle performance at elevated temperatures.* Journal of Alloys and Compounds, 2021. **862**: p. 158022.
26. Zhang, S.S., X. Fan, and C. Wang, *Enhanced electrochemical performance of Ni rich layered cathode materials by using LiPF6 as a cathode additive.* ChemElectroChem, 2019. **6**(5): p. 1536-1541.
27. Huang, W., et al., *A novel electrolyte additive for improving the interfacial stability of high voltage lithium nickel manganese oxide cathode.* Journal of Power Sources, 2015. **293**: p. 71-77.
28. Zhou, K., et al., *An in-depth understanding of the effect of aluminum doping in high-nickel cathodes for lithium-ion batteries.* Energy Storage Materials, 2021. **34**: p. 229-240.
29. Jamil, S., et al., *Significance of gallium doping for high Ni, low Co/Mn layered oxide cathode material.* Chemical Engineering Journal, 2022. **441**: p. 135821.
30. Sun, Y.K., et al., *A novel cathode material with a concentration gradient for high energy and safe lithium ion batteries.* Advanced Functional Materials, 2010. **20**(3): p. 485-491.
31. Heenan, T.M., et al., *Identifying the origins of microstructural defects such as cracking within Ni rich NMC811 cathode particles for lithium ion batteries.* Advanced Energy Materials, 2020. **10**(47): p. 2002655.
32. Jung, C.H., et al., *New Insight into microstructure engineering of Ni Rich layered oxide cathode for high performance lithium ion batteries.* Advanced Functional Materials, 2021. **31**(18): p. 2010095.
33. Kim, U.H., et al., *Microstructure Engineered Ni Rich Layered Cathode for Electric Vehicle Batteries.* Advanced Energy Materials, 2021. **11**(25): p. 2100884.
34. Du, K., et al., *Progresses in sustainable recycling technology of spent lithium ion batteries.* Energy & Environmental Materials, 2022. **5**(4): p. 1012-1036.
35. Baars, J., et al., *Circular economy strategies for electric vehicle batteries reduce reliance on raw materials.* Nature Sustainability, 2021. **4**(1): p. 71-79.
36. Lu, Y., K. Peng, and L. Zhang, *Sustainable recycling of electrode materials in spent Li-ion batteries through direct regeneration processes.* ACS ES&T Engineering, 2022. **2**(4): p. 586-605.
37. Winslow, K.M., S.J. Laux, and T.G. Townsend, *A review on the growing concern and potential management strategies of waste lithium-ion batteries.* Resources, Conservation and Recycling, 2018. **129**: p. 263-277.
38. Mrozik, W., et al., *Environmental impacts, pollution sources and pathways of spent*

lithium-ion batteries. Energy & Environmental Science, 2021. **14**(12): p. 6099-6121.
39. Peng, Y., et al., *A comprehensive investigation on the thermal and toxic hazards of large format lithium-ion batteries with LiFePO4 cathode.* Journal of hazardous materials, 2020. **381**: p. 120916.
40. Wu, J., A. Mackenzie, and N. Sharma, *Recycling lithium-ion batteries: adding value with multiple lives.* Green chemistry, 2020. **22**(7): p. 2244-2254.
41. Zhao, Y., et al., *A review on battery market trends, second-life reuse, and recycling.* Sustainable Chemistry, 2021. **2**(1): p. 167-205.
42. Tesfaye, F., et al., *Improving urban mining practices for optimal recovery of resources from e-waste.* Minerals Engineering, 2017. **111**: p. 209-221.
43. Windisch-Kern, S., et al., *Recycling chains for lithium-ion batteries: A critical examination of current challenges, opportunities and process dependencies.* Waste Management, 2022. **138**: p. 125-139.
44. Xu, P., et al., *Efficient direct recycling of lithium-ion battery cathodes by targeted healing.* Joule, 2020. **4**(12): p. 2609-2626.
45. Zhu, P., et al., *Direct reuse of aluminium and copper current collectors from spent lithium-ion batteries.* Green Chemistry, 2023.
46. Ma, X., et al., *High-performance graphite recovered from spent lithium-ion batteries.* ACS Sustainable Chemistry & Engineering, 2019. **7**(24): p. 19732-19738.
47. Zheng, X., et al., *A mini-review on metal recycling from spent lithium ion batteries.* Engineering, 2018. **4**(3): p. 361-370.
48. Elwert, T., et al., *Current developments and challenges in the recycling of key components of (hybrid) electric vehicles.* Recycling, 2015. **1**(1): p. 25-60.
49. Lv, W., et al., *A critical review and analysis on the recycling of spent lithium-ion batteries.* ACS Sustainable Chemistry & Engineering, 2018. **6**(2): p. 1504-1521.
50. Nasser, O.A. and M. Petranikova, *Review of achieved purities after li-ion batteries hydrometallurgical treatment and impurities effects on the cathode performance.* Batteries, 2021. **7**(3): p. 60.
51. Sa, Q., et al., *Copper impurity effects on LiNi1/3Mn1/3Co1/3O2 cathode material.* ACS applied materials & interfaces, 2015. **7**(37): p. 20585-20590.
52. Kim, S., et al., *Electrochemical effects of residual Al in the resynthesis of Li [Ni1/3Mn1/3Co1/3] O2 cathode materials.* Journal of Alloys and Compounds, 2021. **857**: p. 157581.
53. Ren, J., et al., *The impact of aluminum impurity on the regenerated lithium nickel cobalt manganese oxide cathode materials from spent LIBs.* New Journal of Chemistry, 2017. **41**(19): p. 10959-10965.
54. Li, Y., et al., *Recycling of spent lithium-ion batteries in view of green chemistry.* Green Chemistry, 2021. **23**(17): p. 6139-6171.
55. Zheng, Y., et al., *Unveiling the influence of carbon impurity on recovered NCM622 cathode material.* ACS Sustainable Chemistry & Engineering, 2021. **9**(17): p. 6087-6096.
56. Zhang, R., et al., *Valence Effects of Fe Impurity for Recovered LiNi0. 6Co0. 2Mn0. 2O2 Cathode Materials.* ACS Applied Energy Materials, 2021. **4**(9): p. 10356-10367.
57. Zhang, R., et al., *Understanding fundamental effects of Cu impurity in different forms for recovered LiNi0. 6Co0. 2Mn0. 2O2 cathode materials.* Nano Energy, 2020. **78**: p. 105214.
58. Yang, D., et al., *An efficient recycling strategy to eliminate the residual "impurities" while heal the damaged structure of spent graphite anodes.* Green Energy & Environment, 2022.
59. Huang, B., et al., *Layered cathode materials: Precursors, synthesis, microstructure,*

electrochemical properties, and battery performance. Small, 2022. **18**(20): p. 2107697.
60. Piana, M., et al., *A new promising sol–gel synthesis of phospho-olivines as environmentally friendly cathode materials for Li-ion cells.* Solid State Ionics, 2004. **175**(1-4): p. 233-237.
61. Qin, X., et al., *Mechanism for hydrothermal synthesis of LiFePO4 platelets as cathode material for lithium-ion batteries.* The Journal of Physical Chemistry C, 2010. **114**(39): p. 16806-16812.
62. Ju, S.H. and Y.C. Kang, *The characteristics of Ni–Co–Mn–O precursor and Li (Ni1/3Co1/3Mn1/3) O2 cathode powders prepared by spray pyrolysis.* Ceramics International, 2009. **35**(3): p. 1205-1210.
63. Van Bommel, A. and J. Dahn, *Analysis of the growth mechanism of coprecipitated spherical and dense nickel, manganese, and cobalt-containing hydroxides in the presence of aqueous ammonia.* Chemistry of Materials, 2009. **21**(8): p. 1500-1503.
64. Beak, M., et al., *Effect of Na from the leachate of spent Li-ion batteries on the properties of resynthesized Li-ion battery cathodes.* Journal of Alloys and Compounds, 2021. **873**: p. 159808.
65. Huang, Z., et al., *Investigation on the effect of Na doping on structure and Li-ion kinetics of layered LiNi0. 6Co0. 2Mn0. 2O2 cathode material.* Electrochimica Acta, 2016. **192**: p. 120-126.
66. Ross, G., et al., *Surface modification of poly (vinylidene fluoride) by alkaline treatment1. The degradation mechanism.* Polymer, 2000. **41**(5): p. 1685-1696.
67. Lee, J., et al., *Determining the Criticality of Li Excess for Disordered Rocksalt Li Ion Battery Cathodes.* Advanced Energy Materials, 2021. **11**(24): p. 2100204.
68. MacNeil, D., Z. Lu, and J.R. Dahn, *Structure and electrochemistry of Li [Ni x Co1− 2x Mn x] O 2 (0⩽x⩽ 1/2).* Journal of the Electrochemical Society, 2002. **149**(10): p. A1332.
69. Lu, Z., D. MacNeil, and J. Dahn, *Layered cathode materials Li [Ni x Li (1/3− 2x/3) Mn (2/3− x/3)] O 2 for lithium-ion batteries.* Electrochemical and Solid-State Letters, 2001. **4**(11): p. A191.
70. Wang, H., et al., *Facile fabrication of ethoxy-functional polysiloxane wrapped LiNi0. 6Co0. 2Mn0. 2O2 cathode with improved cycling performance for rechargeable Li-ion battery.* ACS Applied Materials & Interfaces, 2016. **8**(28): p. 18439-18449.
71. Ariyoshi, K., M. Tanimoto, and Y. Yamada, *Impact of particle size of lithium manganese oxide on charge transfer resistance and contact resistance evaluated by electrochemical impedance analysis.* Electrochimica Acta, 2020. **364**: p. 137292.
72. Komaba, S., et al., *Study on polymer binders for high-capacity SiO negative electrode of Li-ion batteries.* The Journal of Physical Chemistry C, 2011. **115**(27): p. 13487-13495.

Acknowledgement

석사 과정을 진행하면서 많은 분들의 도움을 받았습니다. 이 글을 통해 감사의 인사를 전하고자 합니다.

우선, 연구 지도를 비롯하여 석사 과정 동안 항상 큰 힘이 되어 주신 오은석 교수님께 진심으로 감사의 말씀을 드립니다. 교수님께서는 무한한 지지와 격려를 주시며 멋진 어른의 모습을 보여주셨습니다. 이러한 모습을 본받아 저 역시 좋은 연구원이자 어른이 될 수 있도록 노력하겠습니다. 또한 연구와 과제 수행에 많은 협조와 도움을 주신 권의혁 소장님을 비롯한 ㈜코스모화학 관계자 여러분께도 깊은 감사의 인사를 전합니다.

2020년 1월 실험실에 처음 들어왔을 때부터 제게 장비 사용법부터 실험 설계법까지 꼼꼼하게 가르쳐 주신 크리스탈 박사님과 냠카 연구원님께도 깊은 감사의 말씀을 드립니다. 또한 바쁜 일정에도 불구하고 연구 진행에 도움을 주신 에너지 나노 소재 연구실 선배님, 후배님들과 임경조 실장님께도 진심으로 감사의 말씀을 전합니다. 학부 과정을 병행하며 강도 높은 실험 일정을 잘 따라와 멋진 경험을 함께 해준 COTN팀 팀원들에게도 진심으로 감사의 인사를 전합니다.

갑작스러운 대학원 진학 결정을 응원해주시고 지원해주신 저의 부모님과 여동생 그리고 외할아버지께도 깊은 감사의 인사를 전합니다. 덕분에 다른 걱정없이 학교 생활에 집중할 수 있었습니다.

마지막으로, 석사 과정 첫 학기부터 항상 제 옆에서 힘이 되어주고 흔들리지 않게 해준 제 여자친구 정세영과 그 가족분들께도 깊은 감사의 말씀을 드리고 싶습니다.

지면 상에서 언급하지 못했지만, 저를 아끼고 격려해 주셨던 모든 분들께 진심으로 감사의 말씀을 전합니다. 여러분의 아낌없는 지지와 격려가 저에게 큰 힘이 되었습니다. 앞으로도 더욱 열심히 연구하고 발전하여 사회에 도움이 되는 사람으로 성장해 나가겠습니다.

2023년 8월

김재권 올림.